Clays Clay Miner., Vol. 71, No. 1:74–90, 2023
https://doi.org/10.1007/s42860-023-00226-8

ORIGINAL PAPER

Catalytic Reduction of Congo Red to Low-Toxicity Forms Using a Low-Cost Catalyst Based on Modified Bentonite Material

Mehdi Zahraoui · Adel Mokhtar · Zohra Aouali Kebir Medjhouda · Soumia Abdelkrim · Bouhadjar Boukoussa · Amal Djelad · Mohammed Abdelkrim Hasnaoui · Mohamed Sassi · Mohamed Abboud

Accepted: 17 March 2023 / Published online: 20 April 2023

Abstract The reduction of azo dyes to less toxic and more easily biodegradable amine derivatives is an effective strategy for the treatment of industrial wastewater. The present work aimed to study the reduction reaction of azo dye Congo red (CR) catalyzed by nanoparticles (NPs) of chromium oxides (Cr_2O_3NPs) immobilized on bentonite in the presence of $NaBH_4$. Cr(III) ions were intercalated using ion exchange reactions to obtain Cr-bentonite, and then the immobilized chromium cations were treated using $NaBH_4$ leading to the formation of Cr_2O_3NPs-bentonite. The physicochemical properties of the samples were investigated using X-ray diffraction (XRD), scanning electron microscopy/energy dispersive spectroscopy (SEM-EDS), atomic absorption spectrometry (AAS), UV–Visible diffuse reflectance (UV–Vis DR), and Fourier-transform infrared (FTIR) spectroscopy techniques. The results showed the formation of various chromium species, in which the most dominant were chromium oxide nanoparticles, on the bentonite surface with an average particle size between 20 and 35 nm. Line-scan analysis showed a reactive catalytic surface due to the excellent distribution of Cr on the bentonite surfaces. The best-performing catalyst, Cr_2O_3NPs-bentonite, displayed significant catalytic activity compared to the bentonite and Cr-bentonite materials, with a full reduction time of 630 s and a rate constant, k_{app}, equal to 0.034 s^{-1}. The resulting products (benzidine and sodium 3, 4-diaminonaphthalene-1-sulfonate) from the catalytic reduction exhibited low toxicity compared to the CR dye; these products are easy to use in chemical synthesis. All results collected from this work indicated that this low-cost catalyst can be exploited to eliminate other dyes from the environment.

Associate Editor: Jun Kawamata

Supplementary Information The online version contains supplementary material available at https://doi.org/10.1007/s42860-023-00226-8.

M. Zahraoui · A. Mokhtar (✉)
Département Génie Des Procédés, Faculté Des Sciences Et Technologies, Université de Relizane, 48000 Relizane, Algeria
e-mail: mokhtar.adel80@gmail.com

M. Zahraoui · A. Mokhtar · Z. A. K. Medjhouda · S. Abdelkrim · B. Boukoussa · A. Djelad · M. A. Hasnaoui · M. Sassi
Laboratoire de Chimie Des Matériaux L.C.M., Université Oran1 Ahmed Ben Bella, BP 1524, El-Mnaouer, 31000 Oran, Algeria

B. Boukoussa
Département de Génie Des Matériaux, Faculté de Chimie, Université des Sciences et de la Technologie Mohamed Boudiaf, BP 1505, El-Mnaouer, 31000 Oran, Algeria

M. Abboud
Catalysis Research Group (CRG), Department of Chemistry, College of Science, King Khalid University, P.O. Box 9004, Abha 61413, Saudi Arabia

Keywords Bentonite · Catalytic reduction · Chromium oxide nanoparticles · Congo red · $NaBH_4$

Introduction

The presence of synthetic dyes in aquatic systems is a serious environmental problem. These toxic substances are used widely in industry where they are often discharged without treatment (Madhav et al., 2018; Krishnan et al., 2021). Azo dyes (−N=N−) are the most widely used synthetic dyes and constitute the majority of dye production in the world. This type of pollutant has caused severe water pollution which poses a significant threat to human health. In addition to this azo group, they also contain sulfonic ($-SO_3^-$), hydroxyl (−OH), and other electron-withdrawing functional groups, making them less susceptible to degradation. Congo red (CR) belongs to the azo dyes and is abundant in the effluents of the textile and paper industries and has been reported to be extremely carcinogenic and toxic to the environment and to humans (Hudson, 1984). The processing of CR is difficult due to the bulky structure which cannot be degraded easily. Due to the complex nature of textile effluents and the intrinsic properties of this type of dye, therefore, the conventional treatment technologies barely reduce dissolved organic matter and color in textile effluents.

Among the treatment methods, adsorption and catalytic degradation are considered to be the most effective and reliable techniques for the treatment of water containing azo dyes. The adsorption process is characterized by good processing efficiency, ease of use, and relatively low cost; its greatest drawback may be the difficulty in removing contaminants from the adsorbent sample which can saturate its active sites and thus preclude reuse (Vakili et al., 2019). Many toxic dyes can be removed in a short time using catalytic reduction; this results in less toxic products with > 80% conversion even after five cycles of use (Hachemaoui et al., 2021a). The use of economical and low-cost catalysts with large surface areas is essential in catalytic reactions and can also reduce the cost of wastewater treatment.

The activity and selectivity of the nanoparticle-based catalysts in the heterogeneous catalysis reaction depend mainly on the metallic particle size (Hachemaoui et al., 2021b; Abdelkrim et al., 2022; Asli et al., 2022; Mekki et al., 2022). Metal nanoparticles are better for extreme activity due to their various geometric and electronic properties. Synthesis of finely divided metal particles involves the dispersion of the metal catalyst on an inert support. Many materials such as silica, alumina, carbon, and also aluminosilicates such as zeolites and mesoporous materials have been used as supports for the dispersion of the metal particles (Singh et al., 2020; Zhang et al., 2022).

Cr(VI) is one of the most harmful metals. Chromium generally exists in its Cr(III) or Cr(VI) state; while Cr(III) is an important essential micronutrient, Cr(VI) is non-essential, harmful to living organisms, and may cause skin problems, lung cancer, kidney and gastric damage, and respiratory tract and eye irritation (Petrović et al., 2023). To reduce these problems, this metal can be dispersed on a solid support and, thus, have its toxicity decreased.

Clay minerals are one variety of natural materials suitable for scientific research into heterogeneous catalysis (Cheng et al., 2008; De León et al., 2008; Li et al., 2011; Kaur & Kishore, 2012). In recent years, phyllosilicate minerals have attracted the interest of scientists in numerous disciplines, including catalysis (Joseph et al., 2019; Tharmaraj et al., 2022), environmental science (Avila et al., 2021; Imanipoor et al., 2021; Teğin & Saka, 2021), biology, and human health (Carretero, 2002; Carretero et al., 2006; Gomes & Silva, 2007; Abdelkrim et al., 2020; Mokhtar et al., 2020). This interest is generally due to the interesting properties of the clay minerals, including large adsorption capacity, resistance to mechanical forces, large specific surface area, large cation exchange capacity, and swelling in the presence of water (Carretero et al., 2006). These beneficial properties, combined with their wide availability and low cost (Alexander et al., 2019), make them the preferred material for wastewater treatment.

Bentonite is an ore that is widely available and has very large clay content, consisting primarily of montmorillonite (Mnt). It is created by natural weathering of volcanic ash. Its crystal structure comprises an arrangement of aluminosilicate layers each composed of two tetrahedral silica sheets between which is inserted an octahedral aluminum sheet in a 2:1 (tetrahedral-octahedral-tetrahedra, TOT) configuration. An interlayer space containing water and sodium and/or calcium cations separates adjacent layers. These exchangeable cations

https://doi.org/10.1007/s42860-023-00226-8 Published online by Cambridge University Press

counterbalance the negative charge of the aluminosilicate layer, giving the Mnt important properties such as cation exchange capacity (CEC), swellability in water, and space to accommodate within it various other inorganic and organic molecules and cations. These properties make Mnt suitable for a variety of applications. In medicine, for example, it is used in agents for sustained drug release (Park et al., 2016; Hosseini et al., 2018). Due to its specific nature and non-toxicity, the ingestion of the phyllosilicates (e.g. Mnt), which carry the drug molecule, does not impede the relief of gastrointestinal ailments or the curing of infectious diseases (Jlassi et al., 2017). Clay minerals have generated considerable interest in their use as carriers of inorganic compounds and have been confirmed to have a positive impact on the formation and auxiliary stability of metallic nanoparticles. The characteristics described above open many more fields of potential application of these natural materials (Andrades et al., 2004; Ansari Mojarad et al., 2020).

The present study aimed to develop a simple method to produce a Cr_2O_3NPs-bentonite composite as a low-cost and eco-friendly catalyst. The hypothesis was that this could be done by the chemical reduction of Cr(VI)-exchanged bentonite. Another objective was to evaluate the catalytic reduction performance and the recyclability of the catalyst.

Experimental

Materials

The natural bentonite was obtained from the Hammam Boughrara deposit in western Algeria. This material has a cation exchange capacity (CEC) of 80 meq/100 g and a chemical composition already described (Korichi et al., 2009). Cr(III) nitrate nonahydrate ($Cr(NO_3)_3$, $9H_2O$, 99%) and sodium tetrahydridoborate ($NaBH_4$, 98%) were purchased from Sigma-Aldrich (St. Louis, Missouri, USA). Congo red dye ($C_{32}H_{22}N_6Na_2O_6S_2$, CAS number of 573–58-0 and MW 699.66 g/mol) was purchased from Merck Co (Darmstadt, Germany). A representation of the Congo red molecule in 3D format as well as the azo groups is shown in Fig. 1.

Characterization

The X-ray diffraction (XRD) patterns of the samples were recorded using a Bruker AXS D8 Advance X-ray powder diffractometer (Karlsruhe, Germany) with CuKα radiation from 2 to 80°2θ at a scanning rate of 2°/min. Scanning electron micrographs (SEM) and energy-dispersive X-ray spectroscopy (EDS) were obtained using a Thermo Scientific Prisma E scanning electron microscope (Waltham, Massachusetts, USA). Samples were sputter-coated with either gold (Au) or carbon (C). Cr in the leaching test was measured by atomic absorption mass spectrometry (Analytik Jena GmbH—novAA 400 P, Jena, Germany) using a graphite furnace with a detection range of 10–50 ug/L. The calibration solution was Cr/Mg/HNO_3. Fourier-transform infrared (FTIR) spectra were recorded between 4000 and 500 cm^{-1} using a JASCO 4100 spectrometer (Jasco, Japan)(). Ultraviolet–Visible absorbance (UV–Vis) spectra were recorded on a Specord 210 Analytik Jena spectrometer with a holmium oxide filter (Jena, Germany).

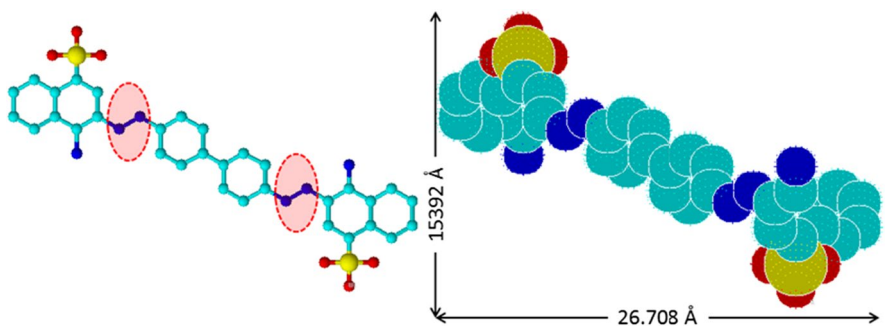

Fig. 1 Chemical structure and size of the CR molecule

https://doi.org/10.1007/s42860-023-00226-8 Published online by Cambridge University Press

Preparation of Catalyst

Prior to the intercalation process, the bentonite was first saturated with Na^+ using a NaCl solution (Arbaoui & Boucherit, 2014; Korichi et al., 2009), which was designed to promote the ion exchange of Cr(III). The saturation process was carried out as follows: 5 g of bentonite was dispersed in deionized water with a minimum resistivity of 18.2 megohm cm and stirred for 30 min at 30°C, then a previously prepared NaCl solution (1 M, 1000 mL) was added to the prepared mixture with vigorous stirring; the new resulting mixture was stirred for 48 h at 30°C, then filtered and washed with deionized water until free of unreacted NaCl. Finally, the Na-saturated solid obtained was dried at 70°C for 72 h.

The dispersion of Cr(III) cations in the interlayer spaces of the Mnt was carried out using an ion-exchange process, and the protocol was as follows: 1.4 g of bentonite was dispersed in deionized water, then the resulting mixture was stirred for 2 h at room temperature (solution A). Cr(III) nitrate solution (100 mL, 0.1 M) was prepared by adjusting the pH to avoid precipitation, and then the solution was added to solution A. After that, the Cr-bentonite material obtained was recovered by filtration, washed thoroughly with distilled water to remove excess unreacted Cr(III) cations, and dried at 70°C for 72 h. The amount of Cr-bentonite material was treated with $NaBH_4$ solution (100 mL, 4 M). The mixture was stirred for 2 h; the final Cr_2O_3NPs-bentonite product was filtered, washed, and dried overnight.

Catalytic Application

Bentonite, Cr-bentonite, and Cr_2O_3NPs-bentonite were evaluated first in order to choose the best catalyst from among them. The catalytic reduction of CR dye in the presence of $NaBH_4$ was carried out under the following conditions: 0.034 g of each catalyst, 0.05 M $NaBH_4$, and 0.06 mM of CR, no solution pH adjustment was made, and the reduction of CR dye was measured in situ by UV–Vis spectroscopy. Firstly, 2.5 mL of CR dye solution was added to 1.5 mL of freshly prepared $NaBH_4$. This solution was transferred to a quartz cuvette to which an amount of catalyst was also added. This system was then loaded into the UV–Vis spectrophotometer and the program was set to scan the sample every 30 s. Afterward, two parameters that affected the catalytic reduction, namely the dose of the catalyst (0.014–0.034 g) and the initial dye concentration (0.06–0.12 mM) were assessed. An adsorption test (dye + catalyst) and a test without catalyst ($NaBH_4$ + dye) were also realized. The kinetics of catalytic dye reduction was investigated by applying the pseudo-first order rate law (Eq. 1 and 2). The percentage degradation of CR dye was also established by using Eq. 3.

$$\frac{dA_t}{dt} = -k_{app}A_t \tag{1}$$

$$\ln\left(\frac{A_t}{A_0}\right) = -k_{app}t \tag{2}$$

where k_{app} (s^{-1}) is the rate constant, A_t is the absorbance at time t, and A_0 is the initial absorbance of the CR dye.

$$\text{Percentage of conversion of CR (\%)} = \frac{A_0 - A_t}{A_0} \times 100 \tag{3}$$

Statistical Analysis

The residual sum of squares (RSS, Eq. 4) measures the accuracy of a regression model. The smaller the residual sum of squares, the better the model fits the data; the greater the residual sum of squares, the less well the model fits the data (Marquardt, 1963).

$$\text{RSS} = \sum_{i=1}^{n} (y_i - fx_i)^2 \tag{4}$$

Results and Discussion

Characterization of Samples

XRD

The structural properties of all prepared samples were examined by XRD analysis. The XRD patterns of bentonite, Cr-bentonite, and Cr_2O_3NPs-bentonite samples (Fig. 2) clearly showed a crystalline structure similar to that of pure Mnt, as described in previous studies, which was confirmed by the presence of reflections (001), (100), (110), and (210) corresponding to Mnt (Cheng et al., 2013). The XRD pattern exhibited

https://doi.org/10.1007/s42860-023-00226-8 Published online by Cambridge University Press

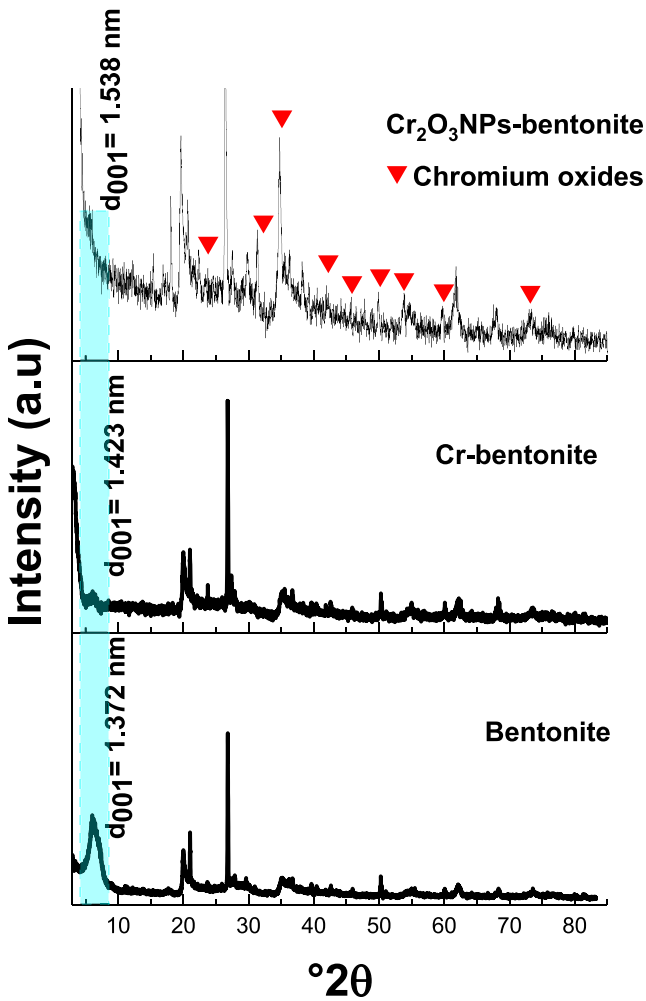

Fig. 2 XRD patterns of bentonite, Cr-bentonite, and Cr_2O_3NPs-bentonite samples

the characteristics (001) peak of Mnt at 6.437°2θ, d_{001} = 1.372 nm. In addition, the diffraction peaks related to quartz, illite, calcite, and K-feldspar impurities were also observed. After the ion-exchange process, the (001) reflection shifted to a lower angle, giving a *d*-spacing of 1.423 nm, which was attributed to the species with a smaller ionic radius being replaced by the species with a larger ionic radius, indicating successful intercalation of Cr(III) cations in the interlayer spaces of montmorillonite. After the chemical treatment using $NaBH_4$ the *d*-spacing was then increased to 1.538 nm. This was probably due to the agglomeration of chromium oxide species on the surface of the bentonite. The characteristic peaks for chromium oxide (at 24.73, 32.62, 35.30, 39.74, 41.64, 45.35, 50.28, 54.89, 59.16, and 73.27°2θ, corresponding to the (012), (104), (110), (113), (202), (024), (116), (214), (300), and (101) planes (Almontasser & Parveen, 2020; Khan et al., 2021), respectively, were observed with low intensities, indicating that the Cr_2O_3NPs were highly dispersed on the bentonite support. This result implies the formation of the rhombohedral structure of chromium in the interlayer spaces of bentonite. By using the Scherrer equation (Eq. 5) (Patterson, 1939), the average particle diameter was calculated and found to be between 35 and 40 nm.

$$\text{The mean size of particles } (\tau) = \frac{K\lambda}{\beta \cos \theta} \quad (5)$$

https://doi.org/10.1007/s42860-023-00226-8 Published online by Cambridge University Press

where τ is the crystallite size (nm); $K = 0.9$, the shape factor; λ (= 0.154060 nm), the wavelength of Cu-Kα radiation; β, the integral breadth of the most intense peak (FWHM); and θ, the diffraction angle.

SEM and EDS

SEM–EDS analysis was used to study the surface morphology and the elemental constituents of the samples. The SEM images of Cr-bentonite and Cr_2O_3NPs-bentonite samples (Figs. 3a,b and 4a,b, respectively) confirmed the conservation of the structure of the Mnt even after the ion-exchange process and the chemical treatment with $NaBH_4$. All micrographs showed the same morphology, which corresponds to the presence of aggregates of ancillary minerals in the bentonite (supplementary information Fig. S1); these are heterogeneous in size and have irregularly shaped cavities, similar results to those found by Cheng et al. (2013).

The EDS spectra of Cr-bentonite and Cr_2O_3NPs-bentonite (Figs. 3c and 4c, respectively) revealed brighter areas, indicating the presence of Cr (Ngah et al., 2012). The brighter areas are because of the better electric conduction properties of chromium compared to the Mnt itself. O, Na, Al, and Si were found in both Cr-bentonite and Cr_2O_3NPs-bentonite, which is not surprising because these are the major components of bentonite. The weight percentages of these elements in Cr-bentonite were O (46.98%), Na (0.69%), Al (10.88%), Si (37.09%), and Cr (4.36%) (Fig. 3, embedded table). For the Cr_2O_3NPs-bentonite, the respective weight percentages were O (43.53%), Na (7.26%), Al (9.05%), Si (33.76%), and Cr (6.40%) (Fig. 4). The increase in Na weight was due to chemical treatment with $NaBH_4$, and the increase in Cr was due to the transformation of Cr(III) to chromium oxide nanoparticles which were dispersed homogeneously on the bentonite surfaces. In addition, the peaks situated at binding energies of 0.5, 5.4, and 5.9 eV indicated the existence of diverse chromium species. Following the element map scan (Figs. 3d and 4d), Cr was clearly intercalated homogeneously on the bentonite. EDS line scan analysis (Fig. 5) was carried out in order to examine the elemental distribution on the Cr-bentonite surfaces; it was distributed homogeneously. That sample thus provided a well dispersed Cr oxide system with a highly reactive catalytic surface. Cr in the Cr_2O_3NPs-bentonite (Fig. 6) was, therefore, uniformly and homogeneously distributed across the whole sample surface and produced a catalytic surface with uniform, active sites.

UV–Vis DR

UV–Vis DR spectroscopy was used to identify the chemical environment and coordination states (Fig. 7) and a large characteristic band in the region of 200–365 nm was revealed and attributed to Al–O and Si–O bonding in the Mnt layers. UV–Vis spectra of the modified Cr-bentonite and Cr_2O_3NPs-bentonite samples indicated the presence of two absorption peaks at 413 and 596 nm, which can be attributed to the presence of several Cr species. In addition, the peak intensity at 314 nm of Cr_2O_3NPs-bentonite was much greater than for the Cr-bentonite. This was due to the transformation of Cr ions to chromium oxide nanoparticles (Ahmad et al., 2018). In addition, deconvolution of the UV–Vis spectra of the Cr_2O_3NPs-bentonite (Fig. S2) confirmed the presence of the $^4A_{2g} \rightarrow {}^4T_{1g}$ transition of the six-coordinate geometry at 413 nm and the $^4A_{2g} \rightarrow {}^4T_{2g}$ transition of chromium ions in an octahedral environment at 596 nm (Liang et al., 2014, 2015).

The CR dye also was characterized by UV–Vis spectroscopy and gave characteristic absorption bands of the conjugation throughout the structure and of the azo bond at 492 and 340 nm. Possible reduction products include amino derivatives which have absorption peaks around 284 nm.

FTIR

The FTIR spectrum of bentonite (Fig. 8) is very similar to that of Mnt, as would be expected from the large proportion of Mnt in bentonite (Hayati-Ashtiani, 2011; Ikhtiyarova et al., 2012). The vibration band observed at 3622 cm^{-1} was attributed to the Al–OH stretching of smectites with a large amount of Al in the octahedral sheet. The broad band observed at 3378 cm^{-1} was attributed to intercalated water molecules linked through hydrogen bonds to the terminal silanol groups. The band at 1400 cm^{-1} was attributed to the stretching and bending vibrations of physisorbed water (Hayati-Ashtiani, 2011).The band at 985 cm^{-1} was

https://doi.org/10.1007/s42860-023-00226-8 Published online by Cambridge University Press

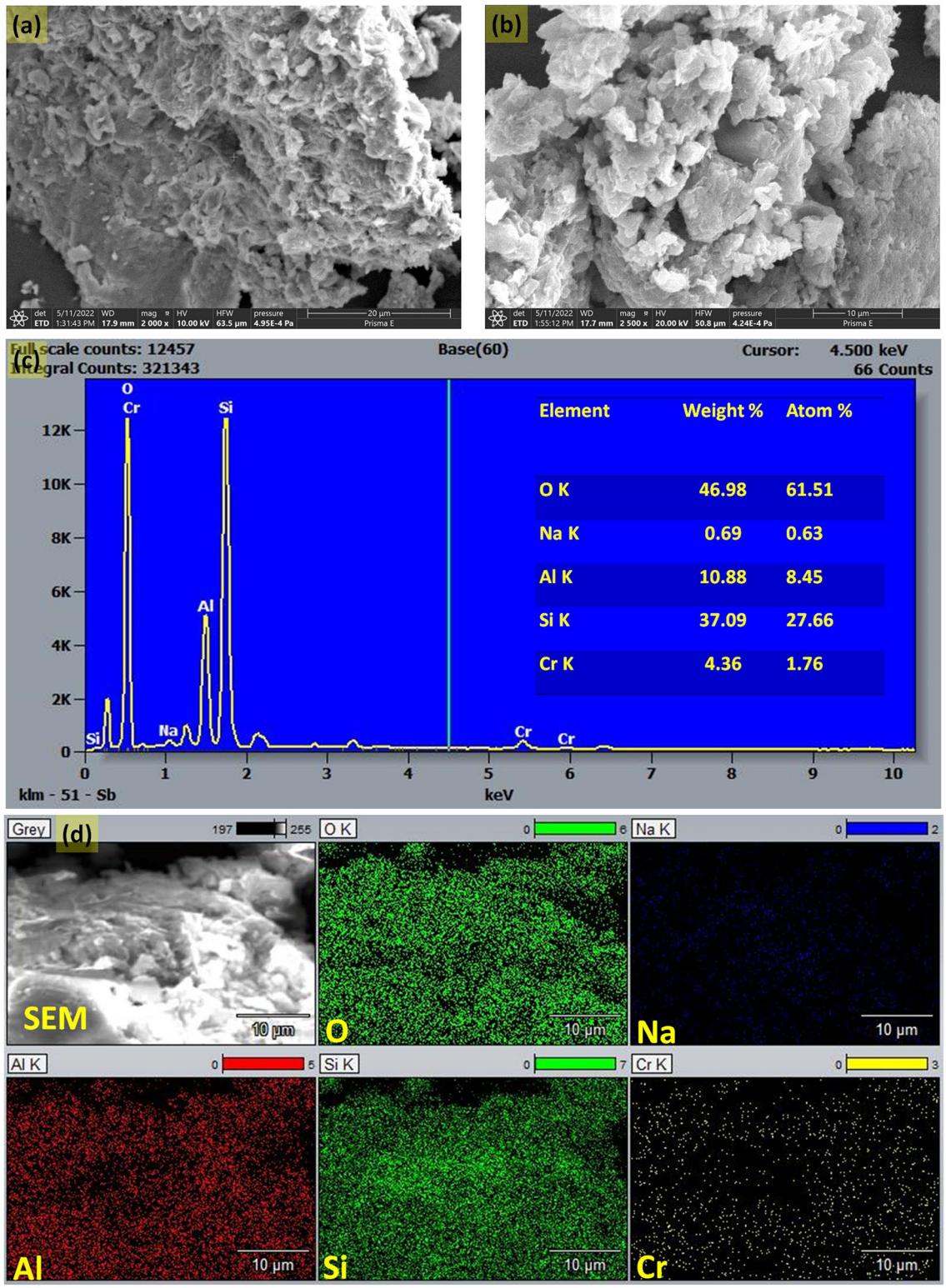

Fig. 3 SEM–EDS analysis of Cr-bentonite: **a-b** SEM images, **c** EDS spectrum, and **d** SEM–EDS element mapping images

https://doi.org/10.1007/s42860-023-00226-8 Published online by Cambridge University Press

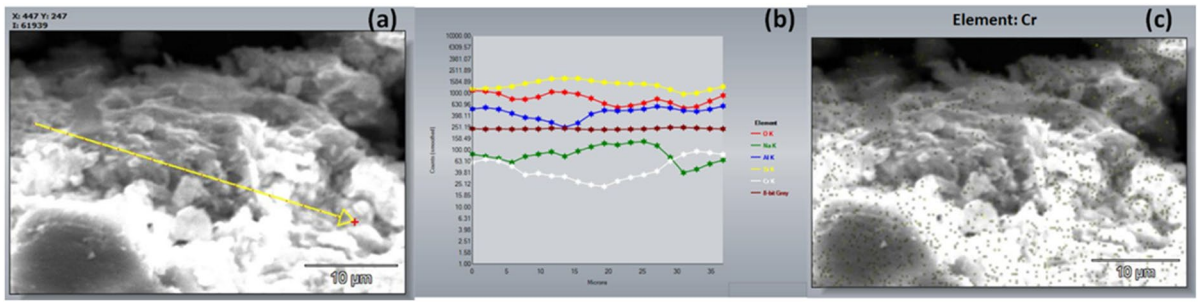

Fig.4 SEM–EDS analysis of Cr_2O_3NPs-bentonite: **a-b** SEM images **c** EDS spectrum, and **d** SEM–EDS element mapping images

attributed to the Si−O stretching vibrations (Madejová & Komadel, 2001); the band at 610 cm^{-1} can be attributed to the bending vibration of the Al−O−Si groups (Aroke et al., 2013; Madejová & Komadel, 2001). The modified materials, Cr-bentonite and Cr_2O_3NPs-bentonite, displayed FTIR spectra that differed in terms of the intensity of the main band as well as the presence of new bands in the latter. The FTIR spectrum of Cr-bentonite showed a decrease in the intensity of the band at 1600 cm^{-1} attributed to the intercalated and physisorbed water molecules, which suggests that the intercalation takes place through an ion-exchange reaction between the Cr(III) ions and the interlayer hydrated sodium cations, thus causing the dehydration of the material obtained after intercalation. The FTIR spectrum of Cr_2O_3NPs-bentonite contained two new bands at 553 and 600 cm^{-1} which were attributed to M−O (Cr−O) stretching (Madi et al., 2007).

Catalytic Study: Selecting the Best Catalyst

Bentonite, Cr-bentonite, and Cr_2O_3NPs-bentonite samples were evaluated as catalysts for CR dye reduction in the presence of $NaBH_4$ as a reducing agent. The respective UV–Vis spectra of the reactions of CR (Fig. 9a,b,c) revealed that the characteristic absorption band of CR at 492 nm was decreased after contact with each catalyst sample. The reduction of CR was incomplete in the presence of bentonite and Cr-bentonite, however, whereas in

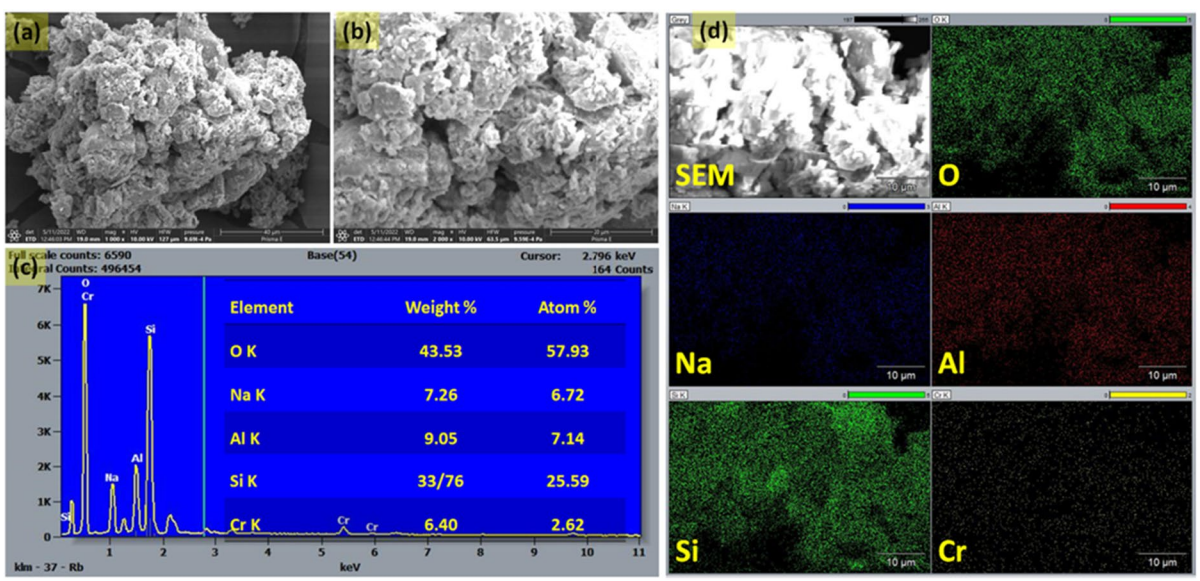

Fig. 5 SEM–EDS analysis of Cr-bentonite: **a-b** line scans of elements and **c** distribution of Cr

https://doi.org/10.1007/s42860-023-00226-8 Published online by Cambridge University Press

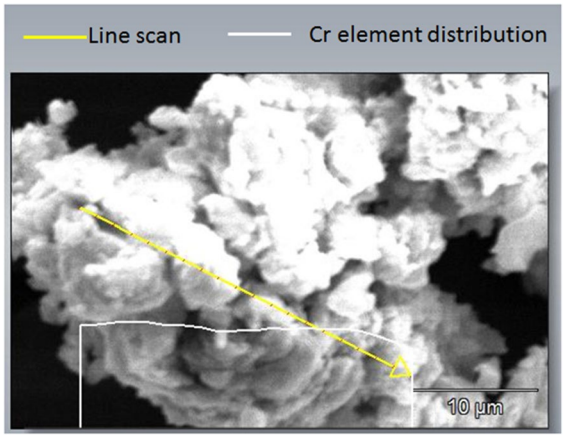

Fig. 6 SEM image and corresponding EDS line scan along the yellow line of the Cr_2O_3NPs-bentonite surface

the presence of Cr_2O_3NPs-bentonite, the reduction reaction was completed after 630 s of contact time. Plots of $\ln(A_t/A_0)$ as a function of reaction time and the catalytic reaction time vs CR dye conversion are given in Figs. 10a and b, respectively. By obtaining UV–Vis spectra of the reaction mixtures at different time intervals, the absorbance at any given wavelength can be plotted vs time. Plotting the change in absorbance with time at a wavelength of $\lambda_{max} = 492$ nm, using the form $\ln(A_t/A_0)$ (Fig. 10a), showed that the absorbance of CR dye decreased with time, indicating that the reduction reaction was on-going. The reaction was incomplete in the presence of bentonite and Cr-bentonite, however, but reached 87.85% of completion after 630 s in the presence of Cr_2O_3NPs-bentonite (Fig. 10b). The Cr_2O_3NPs-bentonite catalyst acted as a charge transfer surface for $NaBH_4$ during the CR reduction reaction, and the reaction became kinetically feasible when the dye molecules were deposited on the Cr_2O_3NPs-bentonite surface. The presence of chromium nanoparticles facilitated the electron transfer that brought about the catalytic reduction of CR dye; the Cr nanoparticles efficiently mediated electron transfer from BH_4^- to azo bonds (Jana & De, 2012). The plot of $-\ln(A_{492})$ vs time (Fig. 10c) demonstrated that the reaction passed through an initial induction period of ~ 100 s during which reagent diffusion was occurring (Benali et al., 2021). After this lag time, the plot became linear and confirmed that the reaction followed a pseudo-first order rate law. The rate constant and regression coefficient were 0.0015 s^{-1} and 0.99, respectively (Table 1). The presence of chromium oxide nanoparticles played an important role in improving the catalytic reduction of CR dye, and thus the most efficient catalyst was

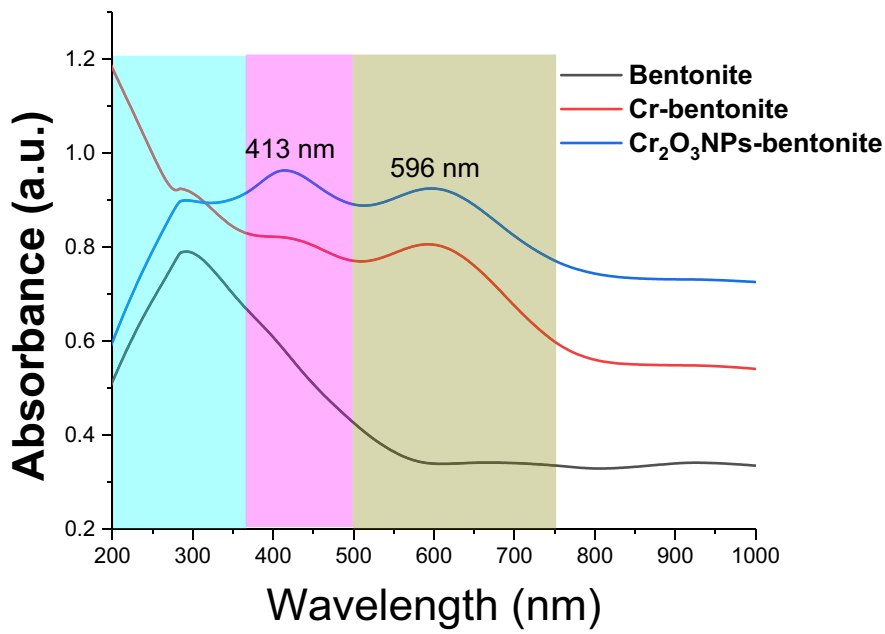

Fig. 7 UV–Vis DR spectra of bentonite, Cr-bentonite, and Cr_2O_3NPs-bentonite samples

https://doi.org/10.1007/s42860-023-00226-8 Published online by Cambridge University Press

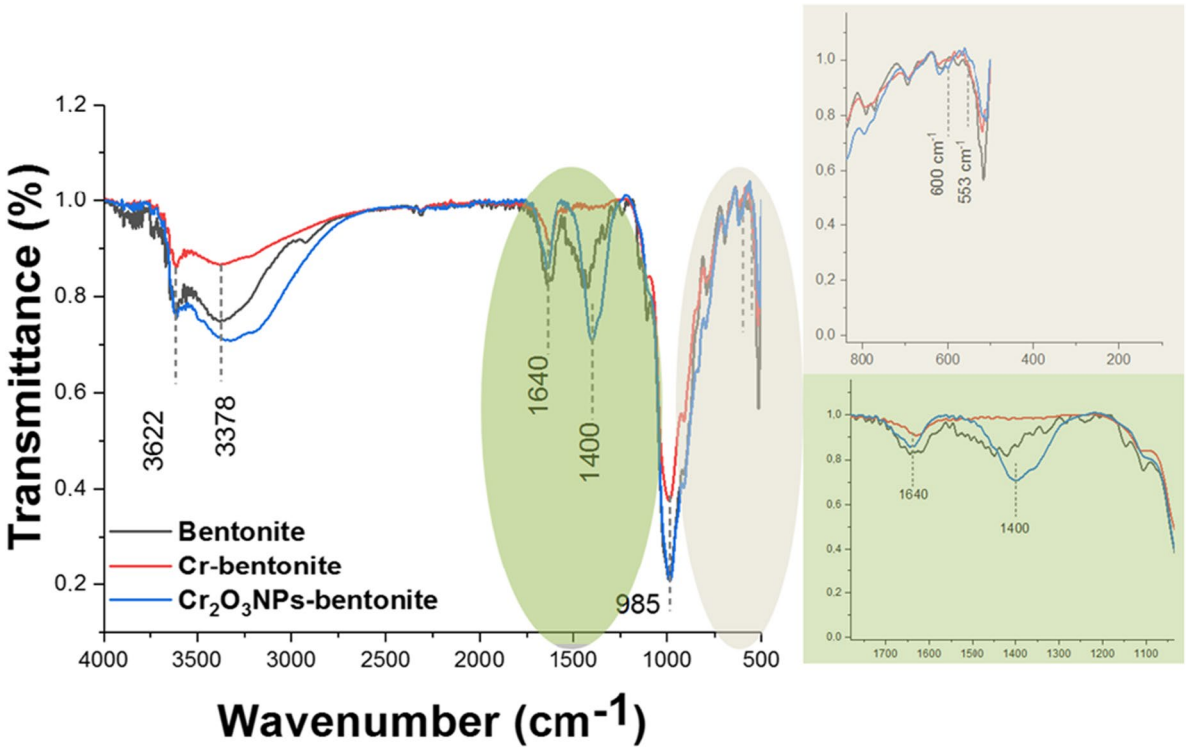

Fig. 8 FTIR spectra of bentonite, Cr-bentonite, and Cr_2O_3NPs-bentonite samples

identified as Cr_2O_3NPs-bentonite, which then was chosen for the rest of this study.

A potential hazard from using a Cr-based catalyst is the leaching of Cr ions into the reaction medium. Leaching tests revealed (Fig. S3) that ~1.1 mg Cr/L was leached from Cr-bentonite whereas only 0.23 mg Cr/L was leached from Cr_2O_3NPs-bentonite.

Variables Affecting the Catalytic Reduction of CR Dye

Firstly, to confirm that both the reductant ($NaBH_4$) and the heterogeneous catalyst (Cr_2O_3NPs-bentonite) were necessary for the CR reduction reaction to occur, the UV–Vis absorbance of CR at $\lambda_{max} = 492$ nm was measured with increasing contact time with the

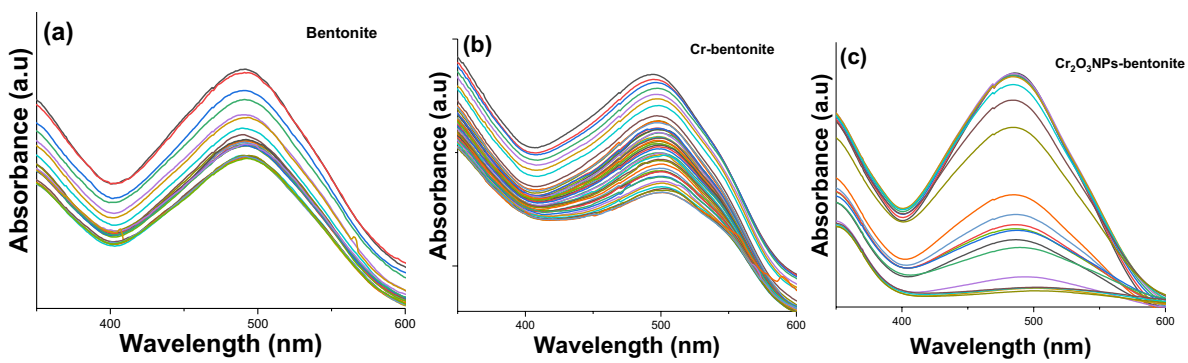

Fig. 9 Time-dependent UV–Vis spectra of CR solution during the catalytic reaction of: **a** bentonite, **b** Cr-bentonite, and **c** Cr_2O_3NPs-bentonite

https://doi.org/10.1007/s42860-023-00226-8 Published online by Cambridge University Press

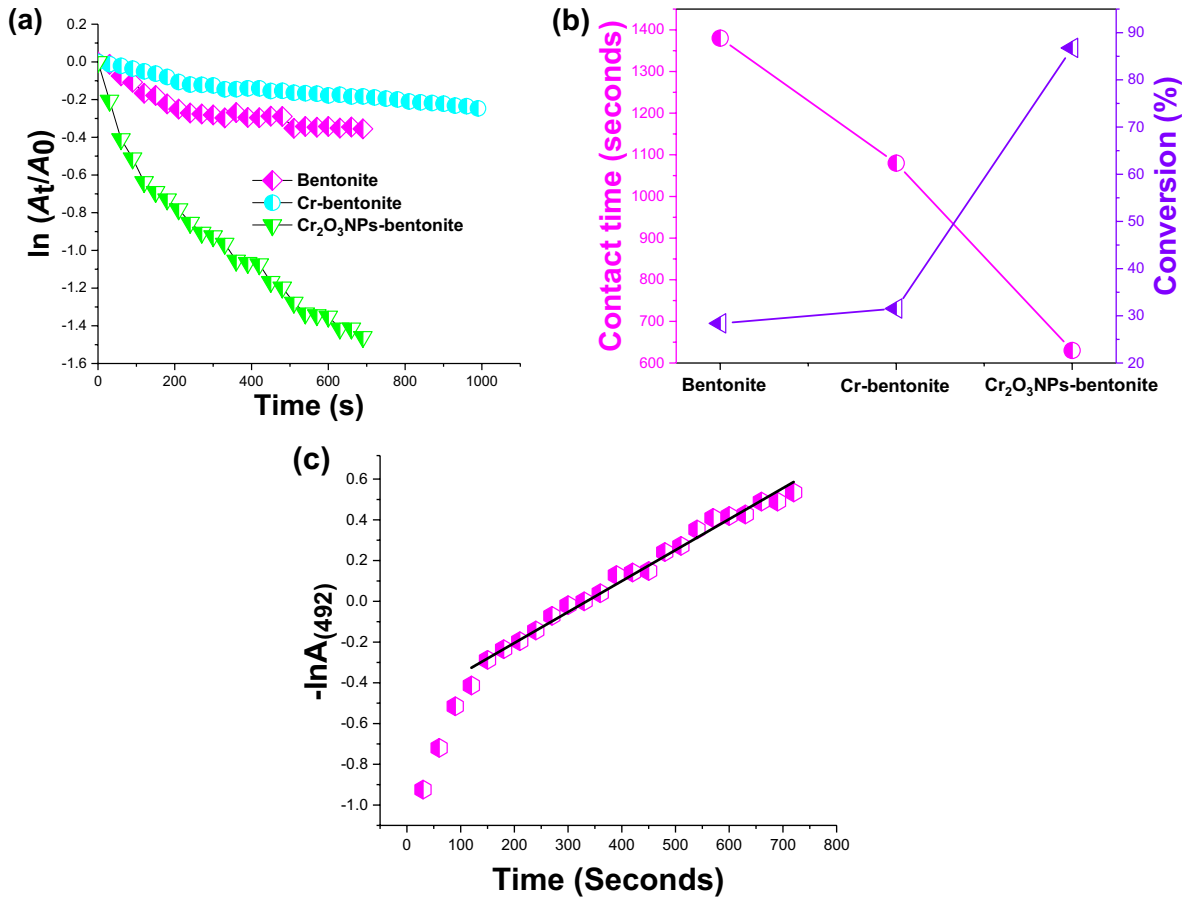

Fig. 10 Study of catalytic reduction of CR dye using bentonite, Cr-bentonite, and Cr_2O_3NPs-bentonite samples in the presence of $NaBH_4$. **a** Plot of $\ln(A_t/A_0)$ as a function of reaction time for CR dye reduction; **b** reaction time and CR dye conversion; and **c** pseudo-first order plot of $-\ln(A_{492})$ (absorbance at 492 nm) vs reaction time, *t*

blank (CR dye + $NaBH_4$) and with catalyst + CR dye (Figs. 11a and b, respectively). Changes in absorbance after as much as 990 s in the presence of the catalyst, but in the absence of the reducing agent, were small (Fig. 11b), thus confirming that little reduction reaction occurred without the reductant. The blank test (Fig. 11a), moreover, revealed that $NaBH_4$ (0.05 M) could achieve only a negligible amount of degradation without the catalyst. Hence, the CR dye reduction is clearly governed by a heterogeneous catalytic reaction (Abdelkrim et al., 2022; Asli et al., 2022).

Table 1 Parameters of the reduction reaction of CR dye

Parameters	Catalyst		
	Bentonite	Cr-bentonite	Cr_2O_3NPs-bentonite
K_{app} (s^{-1})	2.766×10^{-4}	6.531×10^{-4}	0.034
R^2	0.992	0.969	0.981
RSS	0.106	0.391	0.903
Conversion (%)	28.45	31.53	87.85

R^2 coefficient of determination

The effect of Cr_2O_3NPs-bentonite catalyst dose on CR dye degradation was also investigated (Fig. 11c,d). Three masses of Cr_2O_3NPs-bentonite catalyst (0.014, 0.024, and 0.034 g) were used in order to optimize the catalyst dose for CR dye reduction. The plot of $\ln(A_t/A_0)$ as a function of reaction time for CR dye reduction allowed the dose of the catalyst to be correlated with the reaction time and the conversion of the CR dye. The reduction of CR dye neared completion only in the presence 0.034 g

https://doi.org/10.1007/s42860-023-00226-8 Published online by Cambridge University Press

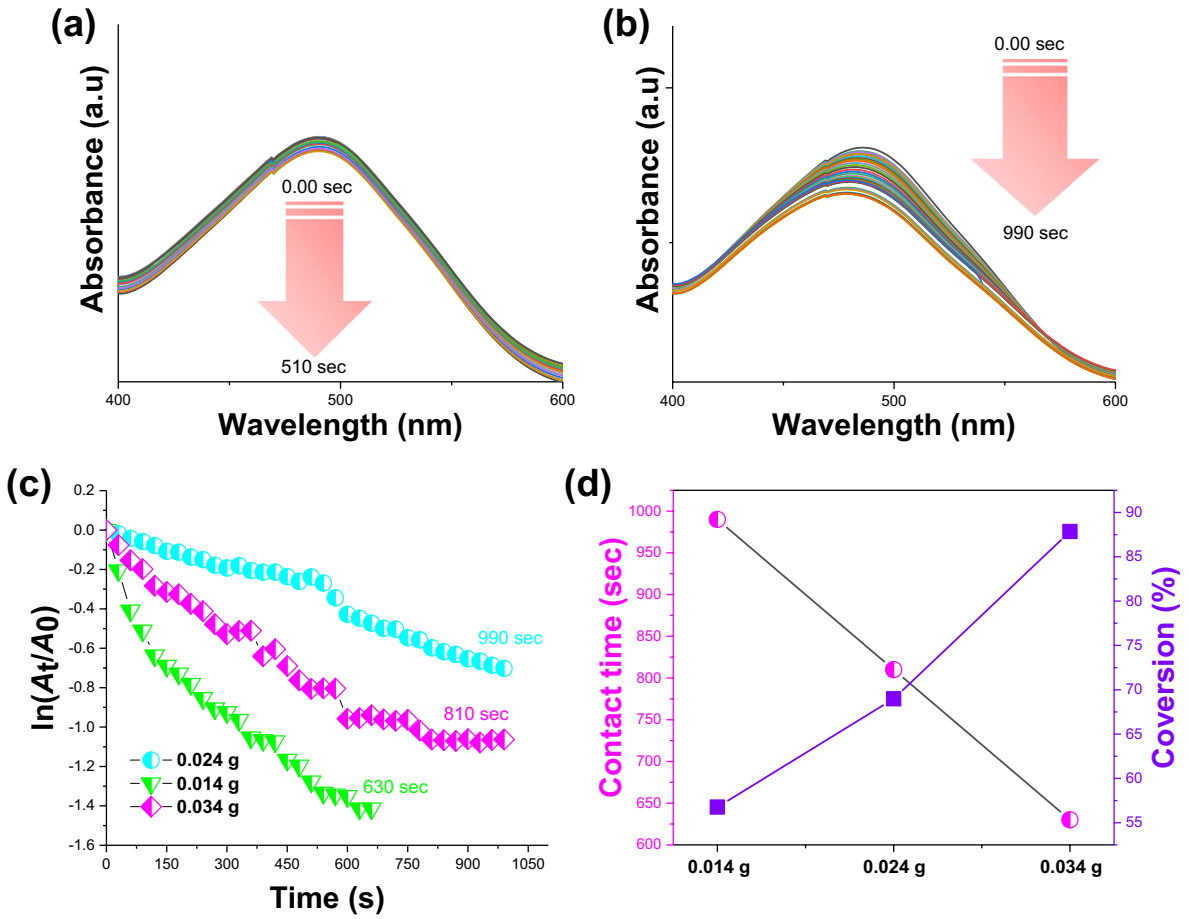

Fig. 11 Study of catalytic reduction of CR dye using three masses (0.014, 0.024, and 0.034 g) of Cr_2O_3NPs-bentonite catalyst. **a** Blank test ($NaBH_4$ + CR dye), **b** adsorption test (catalyst + CR dye), **c** plot of $\ln(A_t/A_0)$ as a function of reaction time for CR dye reduction, and **d** correlation of the dose of the catalyst with the reaction time and the conversion of CR dye

of catalyst compared to the other doses (Fig. 11d). The reduction reaction rate tended to increase with increasing catalyst dose (Fig. 11c); the conversion of dye was also greater for 0.034 g of catalyst dose with a conversion of 87.98% (Fig. 11d). The high catalyst dose provides an abundance of surface-charged Cr_2O_3NPs and, consequently, generates a greater potential for electron transfer and reduces the time required for CR dye reduction.

Two initial dye concentrations (0.06 and 0.12 mM) were also studied to evaluate the performance of the Cr_2O_3NPs-bentonite catalyst. A plot of $\ln(A_t/A_0)$ as a function of contact time (Fig. 12) found that, with a CR concentration of 0.06 mM, the reduction reaction rate was rapid, yielding a total conversion of 87.85% in 630 s, giving a rate constant of 0.034 s^{-1}. When the concentration was 0.12 mM, the reduction reaction took longer and dye conversion was less complete, with a calculated rate constant of 6.76×10^{-4} s^{-1}. With a low dye concentration, the reaction sites on the catalyst are less saturated than when the dye concentration is greater. The greater concentration thus impedes the rate and extent of the conversion reaction.

Plausible Mechanism

A plausible mechanism for the catalytic reduction of CR dye in the presence of $NaBH_4$ is presented in Fig. 13a. The catalytic reaction can reduce the toxicity of CR by converting it to less toxic products. According to this mechanism, in the presence of the catalyst the reducing agent $NaBH_4$

https://doi.org/10.1007/s42860-023-00226-8 Published online by Cambridge University Press

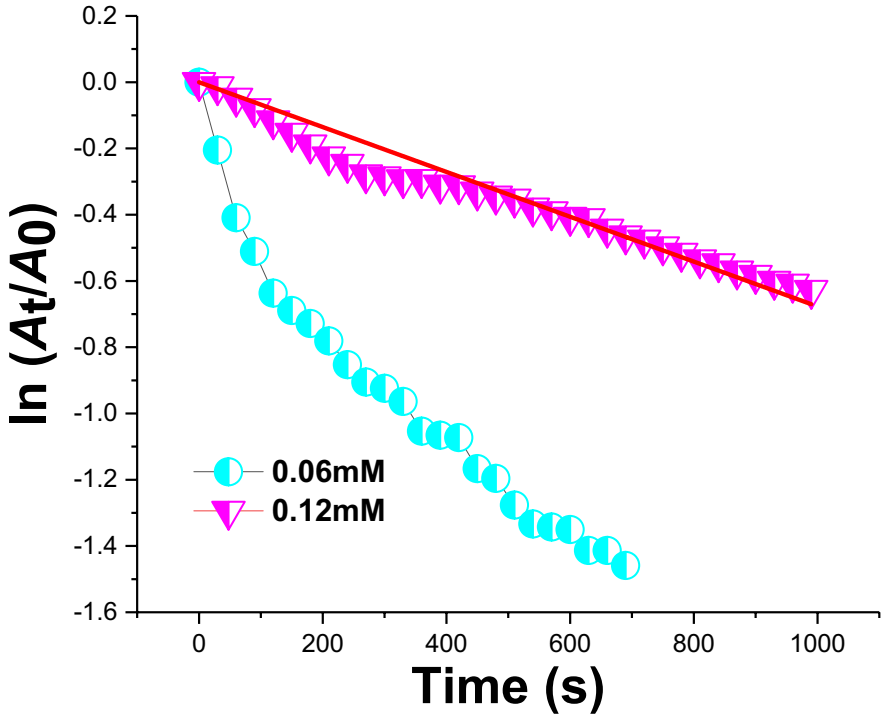

Fig. 12 Change in absorbance of CR with time during catalytic reduction using two initial dye concentrations (0.06 and 0.12 mM)

and the dye molecule are adsorbed on the surface of the solid. Dissociation of the reducing agent to tetrahydroborate ions (BH^{-}_{4}) in the waste solution donates an electron to the catalyst. Then the reduction of water yields hydrogen (H_2), which is a key step for the generation of active hydrogen species at the surface of the catalyst (Bakr et al., 2019). The azo group −N=N− goes through an addition reaction of hydrogen atoms to give a hydrogenated azo intermediate. Then it undergoes further hydrogenation, followed by breaking of the −NH−NH− bond to generate amine derivatives (Naseem et al., 2018; Benmaati et al., 2022), which are less toxic than azo groups.

Progress of the reduction reaction was followed by means of UV–Vis until the band at 492 nm disappeared (Fig. 13b). The results showed that the characteristic CR absorption bands at 492 and 340 nm gradually decreased and a new peak at 284 nm appeared, which is characteristic of the amino derivatives (benzidine and sodium 3, 4-diaminonaphthalene-1-sulfonate) resulting from the reduction products.

Comparison with the Literature

A comparative study (Table 2) of the catalytic activities of various catalysts reported in the literature for the reduction of the CR dye found that most catalysts are based on noble and/or expensive metals, either alone or on supporting materials. In the present study, the supporting material was bentonite, a natural substance that is less expensive than the others listed in Table 2. The Cr_2O_3NPs-bentonite catalyst has a greater rate constant than other catalysts; this means that its catalytic activity is also greater and with a shorter conversion time. Due to the rapid reduction that it promotes, Cr_2O_3NPs-bentonite can be considered to be an effective catalyst for the reduction of environmental pollutants in water.

https://doi.org/10.1007/s42860-023-00226-8 Published online by Cambridge University Press

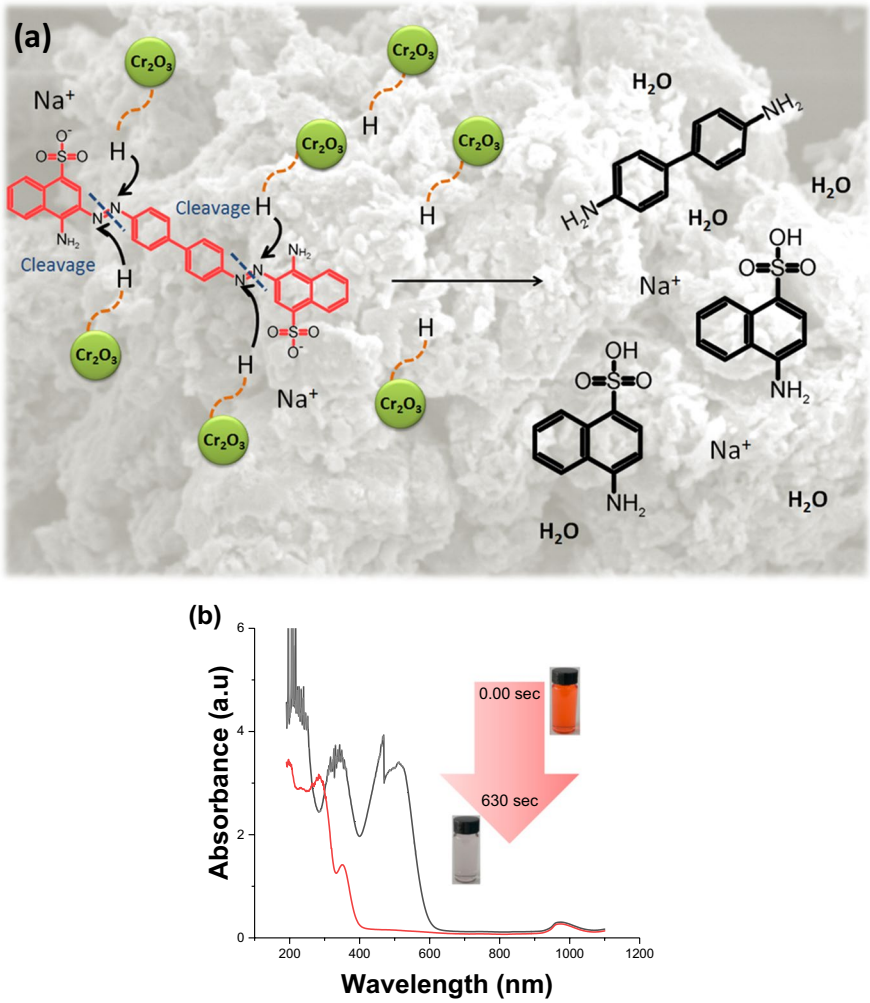

Fig. 13 **a** Plausible mechanism for the reduction of CR dye and **f** the time-dependent UV–Vis spectra for the reduction of CR dye using Cr_2O_3NPs-bentonite

Table 2 Comparisons of the catalytic activities of various catalysts with Cr_2O_3NPs-bentonite for the reduction of CR dye

Catalyst	Reducing agent	Reduction completion time (s)	k_{app} (s^{-1})	References
Ag-pSty-p(NIpmam-AC)	$NaBH_4$	540	$0.63\ 10^{-2}$	(Naseem et al., 2018)
Green synthesis of silver nanoparticles		1080	$1.66\ 10^{-3}$	(Varadavenkatesan et al., 2020)
ZC-Cu		600	0.0045	(Benmaati et al., 2022)
Fe_3O_4-p(AN)-Au NPs		360	0.013	(Chen et al., 2014)
Cr_2O_3NPs-bentonite		630	0.034	Current study

https://doi.org/10.1007/s42860-023-00226-8 Published online by Cambridge University Press

Conclusions

In the present study, the catalytic behavior of low-cost Cr bentonite materials was investigated with respect to the reduction of CR dye. Cr(III) was intercalated into the Mnt layers of the bentonite to obtain Cr-bentonite; it was then treated with $NaBH_4$ to obtain Cr_2O_3NPs-bentonite. Various characterization techniques were applied to verify the presence of chromium nanoparticles. Leaching tests revealed that ~ 1.1 mg Cr/L was leached from Cr-bentonite whereas ~ 0.23 mg Cr/L was leached from Cr_2O_3NPs-bentonite. The catalytic reduction behavior of Cr_2O_3NPs-bentonite was far superior to that of either Cr-bentonite or bentonite alone, in terms of its ability to eliminate 87.85% of the CR dye in 630 s with a rate constant, $k_{app,}$ of 0.034 s^{-1}.

Acknowledgements The authors acknowledge the Deanship of Scientific Research at King Khalid University for funding this work through a research project number RGP.2/226/43.

Data Availability All the data and materials for this study are available herein.

Declarations

Ethics Approval and Consent to Participate Not applicable.

Consent for Publication Not applicable.

Conflict of Interest The authors declare that there is no conflict of interest.

References

Abdelkrim, S., Mokhtar, A., Djelad, A., Bennabi, F., Souna, A., Benguedach, A., & Sassi, M. (2020). Chitosan/ag-bentonite nanocomposites: Preparation, characterization, swelling and biological properties. *Journal of Inorganic and Organometallic Polymers and Materials, 30*, 831–840.

Abdelkrim, S., Mokhtar, A., Djelad, A., Hachemaoui, M., Boukoussa, B., & Sassi, M. (2022). Insights into catalytic reduction of dyes catalyzed by nanocomposite beads alginate@ Fe_3O_4: Experimental and DFT study on the mechanism of reduction. *Colloids and Surfaces A: Physicochemical and Engineering Aspects, 650*, 129595.

Ahmad, Z., Shamim, A., Mahmood, S., Mahmood, T., & Khan, F. U. (2018). Biological synthesis and characterization of chromium (III) oxide nanoparticles. *Engineering and Applied Science Letters, 1*, 23–29.

Alexander, J. A., Ahmad Zaini, M. A., Surajudeen, A., Aliyu, E.-N.U., & Omeiza, A. U. (2019). Surface modification of low-cost bentonite adsorbents—a review. *Particulate Science and Technology, 37*, 538–549.

Almontasser, A. & Parveen, A. Preparation and characterization of chromium oxide nanoparticles. *Proceedings of the AIP Conference Proceedings*, 2020, AIP Publishing LLC, Pp. 020010.

Andrades, M. S., Rodríguez-Cruz, M. S., Sánchez-Martín, M. J., & Sánchez-Camazano, M. (2004). Effect of the modification of natural clay minerals with hexadecylpyridinium cation on the adsorption–desorption of fungicides. *International Journal of Environmental Analytical Chemistry, 84*, 133–141.

Ansari Mojarad, A., Tamjidi, S., & Esmaeili, H. (2020). Clay/starch/Fe_3O_4 nanocomposite as an efficient adsorbent for the removal of methyl violet dye from aqueous media. *International Journal of Environmental Analytical Chemistry, 102*, 1–22.

Arbaoui, F., & Boucherit, M. N. (2014). Comparison of two algerian bentonites: Physico-chemical and retention capacity study. *Applied Clay Science, 91*, 6–11.

Aroke, U., Abdulkarim, A., & Ogubunka, R. (2013). Fourier-transform infrared characterization of kaolin, granite, bentonite and barite. *ATBU Journal of Environmental Technology, 6*, 42–53.

Asli, B., Abdelkrim, S., Zahraoui, M., Mokhtar, A., Hachemaoui, M., Bennabi, F., Ahmed, A. B., Sardi, A., & Boukoussa, B. (2022). Catalytic reduction and antibacterial activity of MCM-41 modified by silver nanoparticles. *Silicon, 14*, 12587–12598.

Avila, M. C., Lick, I. D., Comelli, N. A., & Ruiz, M. L. (2021). Adsorption of an anionic dye from aqueous solution on a treated clay. *Groundwater for Sustainable Development, 15*, 100688.

Bakr, E. A., El-Attar, H. G., & Salem, M. A. (2019). Colloidal ag@ pd core–shell nanoparticles showing fast catalytic eradication of dyes from water and excellent antimicrobial behavior. *Research on Chemical Intermediates, 45*, 1509–1526.

Benali, F., Boukoussa, B., Ismail, I., Hachemaoui, M., Iqbal, J., Taha, I., Cherifi, Z., & Mokhtar, A. (2021). One pot preparation of CeO_2@ alginate composite beads for the catalytic reduction of mb dye: Effect of cerium percentage. *Surfaces and Interfaces, 26*, 101306.

Benmaati, A., Boukoussa, B., Hadjadj Aoul, R., Hachemaoui, M., Kerbadou, R. M., Habib Zahmani, H., & Hacini, S. (2022). Insights into catalytic reduction of organic pollutants catalyzed by nanoparticles supported on zeolite clinoptilolite. *Silicon, 14*, 8831–8843.

Carretero, M. I. (2002). Clay minerals and their beneficial effects upon human health. A Review. *Applied Clay Science, 21*, 155–163.

Carretero, M. I., Gomes, C., & Tateo, F. (2006). Clays and human health. *Developments in Clay Science, 1*, 717–741.

Chen, M., Liu, P., Wang, C., Ren, W., & Diao, G. (2014). Fast catalytic reduction of an azo dye by recoverable and reusable Fe_3O_4@ pani@ au magnetic composites. *New Journal of Chemistry, 38*, 4566–4573.

Cheng, M., Song, W., Ma, W., Chen, C., Zhao, J., Lin, J., & Zhu, H. (2008). Catalytic activity of iron species in

layered clays for photodegradation of organic dyes under visible irradiation. *Applied Catalysis B: Environmental, 77*, 355–363.

Cheng, Y., Zhang, X., Xie, W., Chen, D. & Li, G. (2013) The adsorptive ability of Ti-pillared montmorillonite for lead (II) cations. *Proceedings of the 2013 International Conference on Materials for Renewable Energy and Environment*, pp. 577–580.

De León, M. A., Castiglioni, J., Bussi, J., & Sergio, M. (2008). Catalytic activity of an iron-pillared montmorillonitic clay mineral in heterogeneous photo-Fenton process. *Catalysis Today, 133*, 600–605.

Gomes, Cd. S. F., & Silva, J. B. P. (2007). Minerals and clay minerals in medical geology. *Applied Clay Science, 36*, 4–21.

Hachemaoui, M., Boukoussa, B., Ismail, I., Mokhtar, A., Taha, I., Iqbal, J., Hacini, S., Bengueddach, A., & Hamacha, R. (2021a). CuNPs-loaded amines-functionalized-SBA-15 as effective catalysts for catalytic reduction of cationic and anionic dyes. *Colloids and Surfaces a: Physicochemical and Engineering Aspects, 623*, 126729.

Hachemaoui, M., Mokhtar, A., Ismail, I., Mohamedi, M. W., Iqbal, J., Taha, I., Bennabi, F., Zaoui, F., Bengueddach, A., & Hamacha, R. (2021b). M (M: Cu Co, Cr or Fe) nanoparticles-loaded metal-organic framework mil-101 (Cr) material by sonication process: Catalytic activity and antibacterial properties. *Microporous and Mesoporous Materials, 323*, 111244.

Hayati-Ashtiani, M. (2011). Characterization of nano-porous bentonite (montmorillonite) particles using FTIR and BET-BJH analyses. *Particle & Particle Systems Characterization, 28*, 71–76.

Hosseini, F., Hosseini, F., Jafari, S. M., & Taheri, A. (2018). Bentonite nanoclay-based drug-delivery systems for treating melanoma. *Clay Minerals, 53*, 53–63.

Hudson, M. (1984) Journal of environmental science and health. Part c: Environmental carcinogenesis reviews: Edited by joseph g. Arcos, mary f. Argus and yin-tak woo. Price: Volume 1, number 1, 1983 (2 issues), institutional rate $31.50, individual rate $15.75. Issn: 0736-3001. *Food Chemistry*, *15*, 67.

Ikhtiyarova, G., Özcan, A. S., Gök, Ö., & Özcan, A. (2012). Characterization of natural and organobentonite by XRD, SEM, FT-IR, and thermal analysis techniques and its adsorption behaviour in aqueous solutions. *Clay Minerals, 47*, 31–44.

Imanipoor, J., Mohammadi, M., & Dinari, M. (2021). Evaluating the performance of l-methionine modified montmorillonite k10 and 3-aminopropyltriethoxysilane functionalized magnesium phyllosilicate organoclays for adsorptive removal of azithromycin from water. *Separation and Purification Technology, 275*, 119256.

Jana, D., & De, G. (2012). Controlled and stepwise generation of Cu_2O, Cu_2O@Cu and Cu nanoparticles inside the transparent alumina films and their catalytic activity. *RSC Advances, 2*, 9606–9613.

Jlassi, K., Krupa, I., & Chehimi, M.M. (2017) Overview: Clay preparation, properties, modification. Chapter 1, pp. 1–28 In K. Jlassi, M.M. Chehimi, and S. Thomas (eds.). Clay-Polymer Nanocomposites, Elsevier, https://urldefense.com/v3/__https://doi.org/10.1016/B978-0-323-46153-5.00001-X

Joseph, A., Vellayan, K., González, B., Vicente, M. A., & Gil, A. (2019). Effective degradation of methylene blue in aqueous solution using pd-supported Cu-doped Ti-pillared montmorillonite catalyst. *Applied Clay Science, 168*, 7–10.

Kaur, N., & Kishore, D. (2012). Montmorillonite: An efficient, heterogeneous and green catalyst for organic synthesis. *Journal of Chemistry and Pharmaceutical Research, 4*, 991–1015.

Khan, S. A., Shahid, S., Hanif, S., Almoallim, H. S., Alharbi, S. A., & Sellami, H. (2021). Green synthesis of chromium oxide nanoparticles for antibacterial, antioxidant anticancer, and biocompatibility activities. *International Journal of Molecular Sciences, 22*, 502.

Korichi, S., Elias, A., & Mefti, A. (2009). Characterization of smectite after acid activation with microwave irradiation. *Applied Clay Science, 42*, 432–438.

Krishnan, S.K., Subbiah, K., Kalivel, P. & Subramanian, K. (2021) Degradation of azo dye red me4bl treated with immobilised bimetallic zero-valent iron nanoparticles doped with palladium. *International Journal of Environmental Analytical Chemistry*, 1–12. https://doi.org/10.1080/03067319.2021.2007381

Li, H., Wu, P., Dang, Z., Zhu, N., Li, P., & Wu, J. (2011). Synthesis, characterization, and visible-light photo-fenton catalytic activity of hydroxy Fe/Al-intercalated montmorillonite. *Clays and Clay Minerals, 59*, 466–477.

Liang, S.-T., Zhang, H.-L., Luo, M.-T., Luo, K.-J., Li, P., Xu, H.-B., & Zhang, Y. (2014). Colour performance investigation of a Cr_2O_3 green pigment prepared via the thermal decomposition of CrOOH. *Ceramics International, 40*, 4367–4373.

Liang, S.-T., Zhang, H.-L., Luo, M.-T., Liu, H.-X., Bai, Y.-L., Xu, H.-B., & Zhang, Y. (2015). Preparation of Cr_2O_3-based pigments with high NIR reflectance via thermal decomposition of CrOOH. *Transactions of Nonferrous Metals Society of China, 25*, 2646–2647.

Madejová, J., & Komadel, P. (2001). Baseline studies of The Clay Minerals Society source clays: Infrared methods. *Clays and Clay Minerals, 49*, 410–432.

Madhav, S., Ahamad, A., Singh, P., & Mishra, P. K. (2018). A review of textile industry: Wet processing, environmental impacts, and effluent treatment methods. *Environmental Quality Management, 27*, 31–41.

Madi, C., Tabbal, M., Christidis, T., Isber, S., Nsouli, B. & Zahraman, K. Microstructural characterization of chromium oxide thin films grown by remote plasma assisted pulsed laser deposition. *Proceedings of the Journal of Physics: Conference Series*, 2007, IOP Publishing, Pp. 128.

Marquardt, D. W. (1963). An algorithm for least-squares estimation of nonlinear parameters. *Journal of the Society for Industrial and Applied Mathematics, 11*, 431–441.

Mekki, A., Hachemaoui, M., Mokhtar, A., Issam, I., Bennabi, F., Iqbal, J., Rahmani, K., Bengueddach, A., & Boukoussa, B. (2022). Catalytic behavior and antibacterial/antifungal activities of new mnps/zeolite@ alginate composite beads. *International Journal of Biological Macromolecules, 198*, 37–45.

Mokhtar, A., Bennabi, F., Abdelkrim, S., Sardi, A., Boukoussa, B., Souna, A., Benguedach, A., & Sassi, M. (2020). Evaluation of intercalated layered materials as an antimicrobial and drug delivery system: A comparative study. *Journal of Inclusion Phenomena and Macrocyclic Chemistry, 96*, 353–364.

Naseem, K., Farooqi, Z. H., Begum, R., & Irfan, A. (2018). Removal of congo red dye from aqueous medium by its catalytic reduction using sodium borohydride in the presence of various inorganic nano-catalysts: A review. *Journal of Cleaner Production, 187*, 296–307.

Ngah, W. W., Teong, L., Toh, R., & Hanafiah, M. (2012). Utilization of chitosan–zeolite composite in the removal of Cu (II) from aqueous solution: Adsorption, desorption and fixed bed column studies. *Chemical Engineering Journal, 209*, 46–53.

Park, J.-H., Shin, H.-J., Kim, M. H., Kim, J.-S., Kang, N., Lee, J.-Y., Kim, K.-T., Lee, J. I., & Kim, D.-D. (2016). Application of montmorillonite in bentonite as a pharmaceutical excipient in drug delivery systems. *Journal of Pharmaceutical Investigation, 46*, 363–375.

Patterson, A. (1939). The scherrer formula for x-ray particle size determination. *Physical Review, 56*, 978.

Petrović, R., Lazarević, S., Janković-Častvan, I., Matić, T., Milivojević, M., Milošević, D., & Veljović, Đ. (2023). Removal of trivalent chromium from aqueous solutions by natural clays: Valorization of saturated adsorbents as raw materials in ceramic manufacturing. *Applied Clay Science, 231*, 106747.

Singh, B. K., Lee, S., & Na, K. (2020). An overview on metal-related catalysts: Metal oxides, nanoporous metals and supported metal nanoparticles on metal organic frameworks and zeolites. *Rare Metals, 39*, 751–766.

Teğin, İ. & Saka, C. (2021) Chemical and thermal activation of clay sample for improvement adsorption capacity of methylene blue. *International Journal of Environmental Analytical Chemistry*, 1–12. https://doi.org/10.1080/03067319.2021.1928105

Tharmaraj, V., Vandarkuzhali, S. A. A., Karthikeyan, G., & Pachamuthu, M. (2022). Efficient and recyclable AuNPs@aminoclay nanocomposite catalyst for the reduction of organic dyes. *Surfaces and Interfaces, 32*, 102052.

Vakili, M., Deng, S., Cagnetta, G., Wang, W., Meng, P., Liu, D., & Yu, G. (2019). Regeneration of chitosan-based adsorbents used in heavy metal adsorption: A review. *Separation and Purification Technology, 224*, 373–387.

Varadavenkatesan, T., Selvaraj, R., & Vinayagam, R. (2020). Green synthesis of silver nanoparticles using thunbergia grandiflora flower extract and its catalytic action in reduction of congo red dye. *Materials Today: Proceedings, 23*, 39–42.

Zhang, Q., Gao, S., & Yu, J. (2022). Metal sites in zeolites: Synthesis, characterization, and catalysis. *Chemical Reviews*. https://doi.org/10.1021/acs.chemrev.2c00315